Microarrays of silver nanowires embedded in anodic alumina membrane templates: size dependence of polarization characteristics

Junxi Zhang, Youguo Yan, Xueli Cao, and Lide Zhang

Polarization characteristics of microarrays of silver nanowires embedded in an anodic alumina membrane are theoretically investigated. The microarrays mainly transmit the *p*-polarized wave, whereas they strongly attenuate the *s*-polarized wave in the near- and mid-infrared spectral range. We show that the sizes (e.g., diameter, spacing, and ratio of diameter to spacing) of the nanowires strongly affect the optical losses for the polarized waves. It is predicted that large extinction ratios and small insertion losses can be simultaneously achieved by an appropriate choice of the ratio and the diameter. An optimized design of a nanowire grid polarizer at near- and mid-infrared wavelengths is presented.

OCIS codes: 160.4760, 230.5440, 260.5430.

1. Introduction

Polarization plays a key role in optical devices such as switches, isolators, and modulators. With the development of optical techniques, there are increasing requirements for miniaturization and highly efficient performance of optical polarizing elements. Microoptical polarizing elements have received increased attention owing to their potential applications in optical communications, optical integrated circuits, and orientation detection. In contrast to the conventional metal wire grids fabricated by evaporation[1,2] and lithography[3,4] methods, arrays of metal nanowires can be synthesized through a facile template-based synthesis approach[5] rather than complicated and expensive techniques. As early as 1989, Satio and coworkers proposed a wire grid made of an alumina film, which indicated the polarization performance.[6] In an attempt to improve the polarization properties, ordered arrays of metal nanowires with a onefold size embedded in an anodic alumina membrane (AAM) template have been synthesized successfully,[7] which can work as an efficient wire-grid polarizer at near-infrared wavelengths.

Of particular significance is the size evolution of polarization performance in the metal wire grids. For instance, the first wire grid of copper with a diameter of 1 mm and a spacing of 3 cm was made for a 66 cm radio wave.[1,8] Subsequently the spectral range was further extended from the radio wave to the far-infrared band[9] by use of noble-metal wires 25 μm in diameter. An interesting result was that a wire grid with a wire spacing of 0.463 μm was fabricated by the evaporation of metal on a plastic grating replica,[1] which exhibited the polarization phenomenon at mid-infrared wavelengths. Recently, an aluminum wire-grid polarizer of 0.39 μm wire spacing was fabricated by electron-beam lithography and the lift-off method[3]; the polarization characteristics were demonstrated at the wavelength band of 0.8 μm by an *s*-polarization resonance effect. Moreover, the experiment shows that the *s*-polarization transmittance T_s and the extinction ratio T_s/T_p depend strongly on the width and thickness of the aluminum wires. As the width increases, T_s decreases while T_s/T_p increases; for a fixed width, T_s/T_p increases monotonously with an increase in the thickness of the wires. From the size evolution of the properties, it is clear that metal wire grids with a smaller diameter and spacing will exhibit an efficient polarization phenomenon at shorter wavelengths. In this case, the diameter and the spacing of metal wires can be further reduced to a few nanometers by means of a self-assembly strat-

The authors are with the Key Laboratory of Materials Physics, Institute of Solid State Physics, Chinese Academy of Sciences, 230031 Hefei, China. J. Zhang's e-mail address is jxzhang@issp.ac.cn.

Received 31 May 2005; revised 26 August 2005; accepted 11 September 2005.

0003-6935/06/020297-08$15.00/0

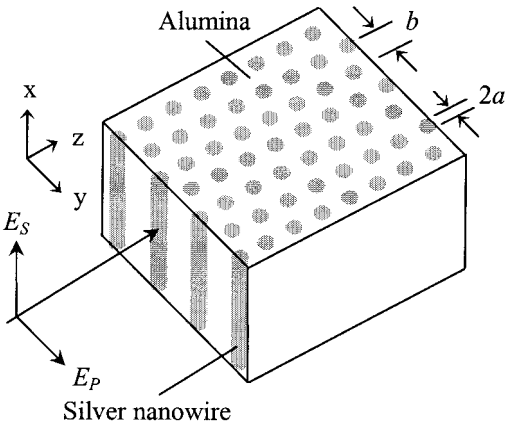

Fig. 1. Schematic illustration of a microarray of silver nanowires embedded in an AAM template.

egy,[10] which can be expected to fabricate an efficient metal wire grid at near-infrared wavelengths, especially the major telecommunication wavelengths (e.g., 1310 and 1550 nm). Our major interest is how to enhance the extinction ratio and reduce the insertion loss of the metallic nanowire arrays at these wavelengths. Therefore a detailed study of the size evolution of polarization properties of arrays is needed. Here, we present a theoretical investigation of polarization characteristics of microarrays of silver nanowires embedded in AAM templates. Both the mechanism of polarization and the effect of the sizes (e.g., diameter, spacing, and ratio of diameter to spacing) on the polarization properties at the near- and mid-infrared wavelengths are explored in detail; we also present a design of a nanowire-grid polarizer at optimum dimensions at the wavelengths investigated.

2. Theory

The microarray shown here is a hexagonally packed nanostructure (Fig. 1), which consists of an ordered arrangement of silver nanowires embedded in an AAM template; the nanowires with a diameter of $2a$ and spacing of b are parallel to each other and perpendicular to the surface of the template.

We consider a light wave that reaches the boundary of the silver nanowires and alumina at normal incidence (as shown in Fig. 1). The wavenumbers k_1 and k_2 can be expressed as $k_1 = 2\pi n_1/\lambda$ and $k_2 = 2\pi n_2/\lambda$; here λ is the wavelength of the incident wave in vacuum, n_1 represents the refractive index of alumina, and the optical constant n_2 (the so-called complex refractive index) of silver can be written[11] as $n_2 = n_s - ik$, where n_s and k are the refractive index and the extinction coefficient, respectively. E_s and E_p are the electric fields of the incident waves, corresponding to light polarized parallel (s polarization) and perpendicular (p polarization) to the nanowire axis. We can determine the optical losses of a row of the nanowires by considering a coupling effect of adjacent nanowires,[12] if we consider a row of the nanochannels of the AAM as fully filled with silver nanowire; then the transmission coefficient is given by

$$t_{if} = 1 - \left(1 - \frac{ib\eta_{1i}}{\pi k_1 a^2}\right)^{-1} - \left[1 + \frac{ik_1 b(\eta_{0i} - \log 2)}{\pi}\right]^{-1}, \tag{1}$$

where $i = s, p$, the subscript f means the full filling of the nanochannels, and η_{0i} and η_{1i} are two parameters dependent on the polarization direction. Furthermore, we can obtain the quantities by using the boundary conditions. For s polarization the parameters take the forms

$$\eta_{0s} = \frac{J_0(k_2a) - (k_2a)J_0'(k_2a)\log(\pi a/b)}{(k_1a)^2 J_0(k_2a)/2 + (k_2a)J_0'(k_2a)}, \tag{2}$$

$$\eta_{1s} = \frac{J_1(k_2a) + (k_2a)J_1'(k_2a)}{J_1(k_2a) - (k_2a)J_1'(k_2a)}. \tag{3}$$

For p polarization, we have

$$\eta_{0p} = \frac{(k_2a)J_0(k_2a)/(k_1a)^2 - J_0'(k_2a)\log(\pi a/b)}{(k_2a)J_0(k_2a)/2 + J_0'(k_2a)}, \tag{4}$$

$$\eta_{1p} = \frac{(k_2a)J_1(k_2a) + (k_1a)^2 J_1'(k_2a)}{(k_2a)J_1(k_2a) - (k_1a)^2 J_1'(k_2a)}, \tag{5}$$

where J_0 and J_1 are Bessel functions of the zeroth and first orders, respectively, and J_0' and J_1' are their corresponding derivatives, respectively.

Previous theoretical treatments were based on a simplified assumption that the nanochannels of an AAM are fully filled with the nanowire when the optical losses of the whole nanowire microarrays are determined.[13] In fact, full filling (100%) of the nanochannels is still a significant challenge via the self-assembly approach,[14] which requires that the nanowire nucleation occur simultaneously in all of the nanochannels, and that the growth rate of the nanowires be uniform to ensure that the nanowires are uniform in length and equal to the thickness of the template. Considering the filling inhomogeneity in fabricating nanowire arrays, a filling fraction of the nanochannels should be incorporated into this theoretical calculation. First, the optical loss per thickness α_{ip} for a partial filling for n rows of nanowires can be expressed as

$$\alpha_{ip} = \frac{V_p}{V_f}\,\alpha_{if}, \tag{6}$$

where $i = s, p$; α_{if} is the loss per thickness for a full filling; and V_p and V_f represent the total volumes of the nanowires with the partial and the full fillings, respectively. At this point, $V_p = m_p\pi a^2 l_p$ and $V_f = m_f\pi a^2 l_f$; here m_p and m_f are the average numbers of the nanowire nucleation for the partial and full fill-

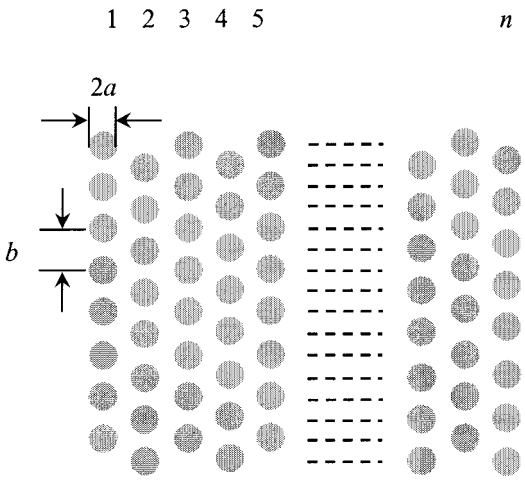

Fig. 2. Schematic drawing of the microarray with n rows of nanowires.

ing, respectively, and l_p and l_f correspond to the average lengths of the nanowires partially and completely filled in the nanochannels, respectively. Equation (6) is now written as

$$\alpha_{ip} = \delta\alpha_{if}, \tag{7}$$

where $\delta = \delta_m\delta_l$, defined by the filling fraction of the nanochannels. In addition, $\delta_m = m_p/m_f$ and $\delta_l = l_p/l_f$, which represent the average percentage of the nanowire nucleation in contrast to the nanochannel number and that of the nanowire length compared with the thickness of the template, respectively.

On the other hand, the optical loss of per-thickness α_{if} of the microarray with n rows of nanowires filled completely into the nanochannels (as shown in Fig. 2) is given by

$$\alpha_{if} = \frac{1}{d}\log\left(\frac{1}{T_{if}^{\,n}}\right), \tag{8}$$

where

$$T_{if} = |t_{if}|^2, \tag{9}$$

$$d = (n-1)(\sqrt{3}/2)b. \tag{10}$$

The extinction ratio L_s and the insertion loss L_p for the partial filling can be defined by $(\alpha_{sp} - \alpha_{pp})d$ and $\alpha_{pp}d$, respectively. Consider the thickness d of 10 μm (the number of rows $n \gg 1$); in terms of Eqs. (7), (8), and (10), we then have

$$L_s = \frac{-20}{\sqrt{3}b}\,\delta(\log T_{sf} - \log T_{pf}), \tag{11}$$

$$L_p = \frac{-20}{\sqrt{3}b}\,\delta \log T_{pf}. \tag{12}$$

3. Results and Discussion

Optical loss spectra of the microarrays can be numerically simulated based on Eqs. (11) and (12). The refractive index n_1 of alumina is obtained from Ref. 15 and the optical constant n_2 of silver is taken from the compilations of Lynch and Hunter.[11]

In general, the diameter and the spacing of the nanowires embedded in the AAM template are consistent with those of the nanochannel of the template for a typical self-assembly process, respectively. Here we demonstrate two configurations of the template to explore the size evolution of polarization characteristics. One template with large-scale nanochannels (e.g., 100 or 130 nm spacing) is prepared by a two-step anodization process in an oxalic acid solution (oxalic acid template)[16,17]; the other with small-scale nanochannels (e.g., 70 nm spacing) is fabricated by means of a similar process in a sulfuric acid solution (sulfuric acid template).[18]

Although it is difficult to determine the filling fraction of the nanochannels for nanowire arrays embedded in an AAM in current experiments, and the filling from Ref. 7 has not been performed either, we can approximately estimate the filling fraction in terms of the actual fabrication[7] and other groups' results similar to those of the experiment. For instance, the investigation of Mössbauer spectra showed a 30% filling fraction for Fe nanowires embedded in an AAM template.[19] Müller *et al.* reported that the filling of silver nanowires in the template is rather low and not continuous when electric force microscopy is used, and they attributed the filling interruption to defects and hydrogen development.[20] A favorite result is that most of the nanochannels can be filled with silver nanowires to 90% in length under a specific pulsed electrodeposition with a constant-current condition.[21] Recently, Stacy's group also explored the filling. They observed the nucleation percentage in 65%–75% for Bi_2Te_3 nanowire arrays prepared by a direct-current (dc) electrodeposition.[14] Furthermore, a high nucleation percentage in 85%–90% of the nanochannels was achieved by use of potentials that were as positive as possible, and the length percentage of $Bi_{1-x}Sb_x$ nanowires was approximately one third of the thickness of the template.[22] Since the status of the template has a profound effect on the nucleation percentage, which includes grain boundaries,[14] structural defects,[20] and channel blockage from impurity adsorption,[23] the nucleation percentage in the previous experiment is estimated as 70%, similar to what Stacy's group reported above in view of a large area of the template.[14] On the other hand, the length percentages of the nanowires are influenced by not only the growth time but also by the growth rate of the nanowires, strongly depending on the electrodeposition conditions such as deposition modes (e.g., dc or pulsed electrodeposition), applied potentials, electrolyte solution, and temperature.[24–26] In the previous experiment, the silver nanowire array embedded in an AAM was prepared by a general dc electrodeposition. In addition, considering an element nanowire

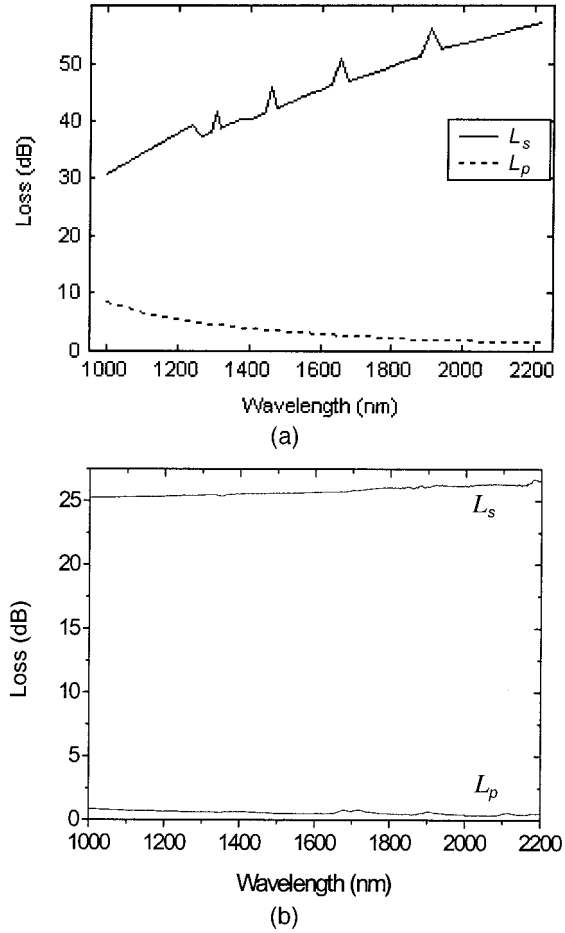

Fig. 3. Optical loss spectra of a microarray of silver nanowires 90 nm in diameter and 130 nm in spacing: (a) theoretical results, (b) experimental data by Pang *et al.*[7]

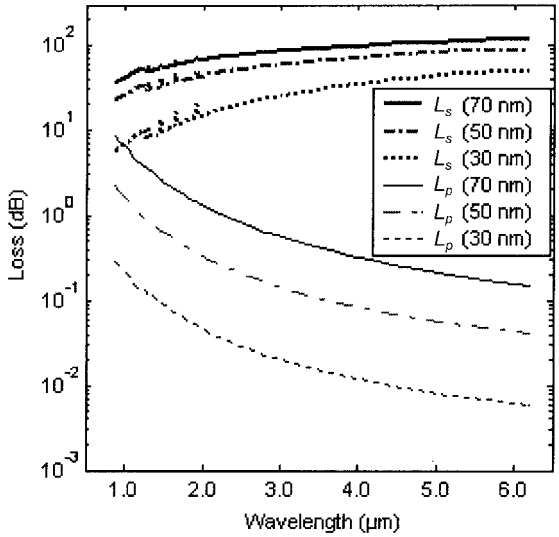

Fig. 4. Diameter dependence of optical loss spectra of silver nanowire microarrays for a fixed spacing of 100 nm.

array compared with the alloy nanowire array from Ref. 22 and fabrication by pulsed electrodeposition,[21] we can approximately evaluate a 60% average percentage of the nanowire length compared with the thickness of the template. As a result, the filling fraction of the nanochannels is estimated at 42% in the experiment.[7]

Compared with the experiment,[7] theoretical loss spectra of a silver nanowire microarray embedded in an AAM are shown in Fig. 3(a). It can be seen that L_s increases while L_p decreases with increasing wavelength, which is in agreement with the experiment [as shown in Fig. 3(b)]. Furthermore, we find several separated peaks at 1240, 1350, 1459, 1653, and 1907 nm in the spectrum of L_s, which possibly originate from those peaks of the complex refractive indexes of silver at the relevant wavelengths, and those are actually observed owing to the data errors selected from Ref. 11. In addition, the peaks at those wavelengths are not obvious in the spectrum of L_p because the peaks have been concealed by the larger values of L_p; nevertheless, those peaks can also be observed in the spectrum with lower L_p, as demonstrated below. On the other hand, both L_s and L_p are still slightly higher than those obtained in the previous experiment when only the filling fraction, which is regarded as a primary factor that affects the optical losses in values, is considered. First, the estimation of the filling fraction is not accurate in view of the concrete experimental conditions in contrast to other groups' similar results. Second, the nanochannels are not perfectly arranged by a hexagonally packed pattern in a large area and the shape of the channels is not completely cylindrical.[18] In these cases, the shape and the ordered degree of the nanochannels perhaps influence the optical losses. Furthermore, the discrepancy is possibly due to the different crystallization and density of the silver nanowires for comparison with those of the films from the compilations.[11]

To achieve the loss spectra in a wider wavelength region, here we extend the spectra range beyond those in the experiment. Figure 4 shows optical loss spectra of microarrays of silver nanowires embedded in the oxalic acid templates with different diameters at near- to mid-infrared wavelengths. Both L_s and L_p increase with an increase in the diameter from 30 to 70 nm. For an *s*-polarized wave propagating along the *z* direction (Fig. 1), a strong Fresnel reflection occurs at discrete interfaces of the nanowires and alumina matrix because of the distinct difference of the optical constants between silver[11] and alumina.[15] In this respect, the increase in the Fresnel reflection with the wavelength is mainly due to the increase in the reflectivity[27] R_F for the *s*-polarized wave at normal incidence, and we write

$$R_F = \frac{(n_s - n_1)^2 + k^2}{(n_s + n_1)^2 + k^2}. \tag{13}$$

In addition, driven by the field E_s along the nanowire axis, the conduction electrons in the metal lose energy both by electron–phonon and electron–lattice

defect interactions, and, in this case, the wave is absorbed. Hence optical loss for *s*-polarization is derived from the Fresnel reflection and the absorption.

On the other hand, for thin nanowires of tens of nanometers in diameter, the electrons driven by the field E_p are not free to move very far (hundreds of nanometers) in the direction perpendicular to the nanowire axis because the mean-free path of the electrons in the metal is close to the nanowire diameter; therefore the field component of the *p*-polarized wave will not change essentially. Because the diameter of the nanowires is very small compared with those wavelengths, the average scattering cross section C_{sca} per cylindrical nanowire can be estimated according to the Rayleigh approximation for *p* polarization[28]; we express the quantity in the form

$$C_{\mathrm{sca}} = \frac{8}{3}\pi k_1^{\,4}|\alpha|^2, \tag{14}$$

where $|\alpha|^2$ is defined by

$$|\alpha|^2 = h^2|\alpha_x|^2 + q^2|\alpha_y|^2 + l^2|\alpha_z|^2; \tag{15}$$

here α_j is the polarizability tensor along the three main axes ($j = x, y, z$) for an ellipsoid (see Fig. 1) and h, q, and l are the direction cosines of E_i ($i = s, p$) with respect to the three main axes of α_j. When considering the ellipsoid particles embedded in the host medium of vacuum,[29] we have

$$\alpha_j = \frac{V}{4\pi}\frac{n_2^{\,2} - 1}{1 + L_j(n_2^{\,2} - 1)}, \tag{16}$$

where L_j are the Lorentz depolarization factors ($L_x + L_y + L_z = 1$) related to the three axes and V represents the volume of one ellipsoid. In terms of the host medium of dielectric (e.g., alumina), the polarizability tensor takes the form

$$\alpha_j = \frac{V}{4\pi}\frac{n_2^{\,2} - n_1^{\,2}}{n_1^{\,2} + L_j(n_2^{\,2} - n_1^{\,2})}. \tag{17}$$

If the nanowire is assumed to be cylindrical, we have $L_x = 0$ and $L_y = L_z = 1/2$. In addition, for *p* polarization, $h = l = 0$ and $q = 1$ in Eq. (15), we note the extinction coefficient $k \gg n_1$ from Eqs. (14), (15), and (17), and the Rayleigh scattering cross section is given by

$$C_{\mathrm{sca}} = 2k_1^{\,4}V^2/3\pi. \tag{18}$$

If we take into account the same irradiation area for the incident waves, the Rayleigh scattering loss L_R is given by

$$L_R \propto m_p\delta_l^{\,2}(a/\lambda)^4. \tag{19}$$

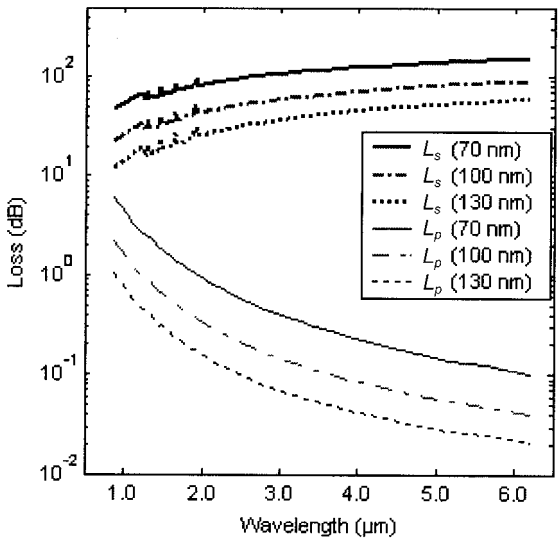

Fig. 5. Spacing dependence of optical loss spectra of silver nanowire microarrays for a fixed value of 50 nm in diameter.

It is found that the insertion losses are approximately consistent with the losses from the Rayleigh scattering (as demonstrated in Fig. 4). Therefore the insertion losses may result from the contribution from Rayleigh scattering by electric dipole radiation.

The optical loss spectra with different diameters can be explained further for fixed spacing (e.g., 100 nm); the number of nanowires is uniform for the same incident area of the waves. There is an increasing amount of metal to reflect and absorb the *s*-polarized wave with increasing diameter; thus L_s increases, while the metal with an increase in fraction takes part in the Rayleigh scattering for *p* polarization, which leads to an enhancement in L_p.

The optical loss spectra with different spacings are displayed in Fig. 5. Both L_s and L_p are found to decrease when the spacing increases from 70 to 130 nm. The number of the nanowire decreases with increasing spacing as the diameter is uniform (e.g., 50 nm), which results in a reduced amount of the metal that reflects and absorbs the *s*-polarized wave, and in this case L_s decreases; similarly, L_p also decreases owing to the reduction of the Rayleigh scattering.

It is worth noting that both L_s and L_p clearly exhibit the same size dependence of polarization characteristics when one quantity (e.g., diameter or spacing) is independently varied, as described above. Nevertheless, the current interest is in how to increase L_s and synchronously diminish L_p in the spectral range. Figure 6 shows the diameter dependence of the optical losses when different ratios of $2a$ to b are chosen (e.g., $2a/b = 0.1$, 0.3, 0.5, and 0.7). A slight increase in L_s is observed with increasing diameter from 7 to 13 nm for $2a/b$ of 0.1 [Fig. 6(a)]; when $2a/b$ is increased further, L_s first increases and then decreases with an increase in the diameter from 21 to 39 nm [Fig. 6(b)]; however, we find a diameter-dependent decrease in L_s when the value of $2a/b$ is 0.5 or larger [Figs. 6(c)

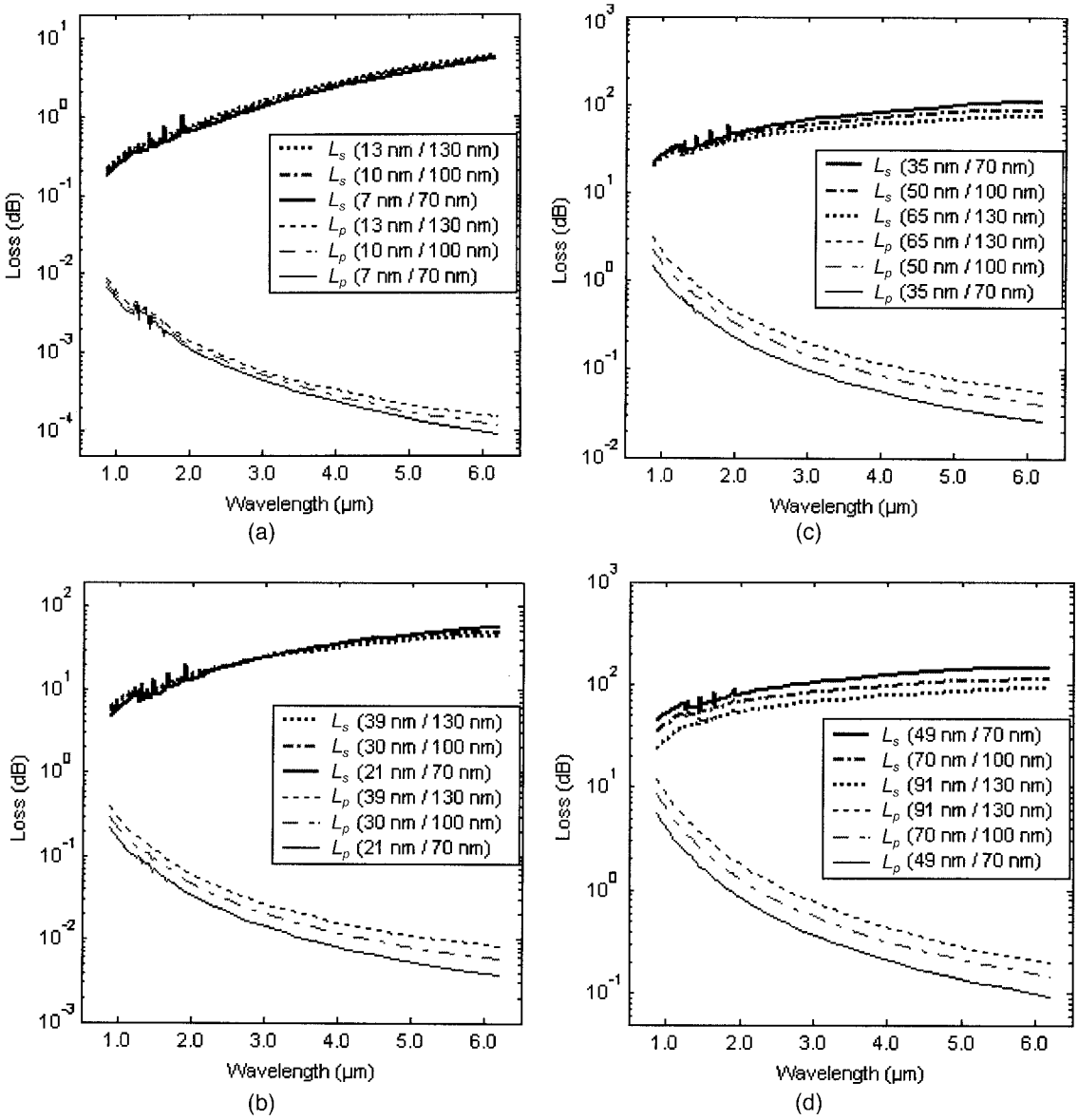

Fig. 6. Diameter evolution of optical loss spectra of the microarrays of silver nanowires when different ratios of $2a$ to b are selected: (a) $2a/b = 0.1$, (b) $2a/b = 0.3$, (c) $2a/b = 0.5$, and (d) $2a/b = 0.7$.

and 6(d)]. On the other hand, L_p is slightly enhanced with increasing diameter for those chosen values of $2a/b$ [see Figs. 6(a)–6(d)]. Furthermore, it is also found that L_p remarkably increases with an increase in the ratio of $2a$ to b from 0.1 to 0.7 for a fixed value of spacing [as shown in Figs. 6(a)–6(d)].

The optical losses with different diameters for those selected values of $2a/b$ can be analyzed as follows: Because both $2a$ and b display a strong influence on the optical loss for s polarization, different contributions of the loss from those quantities will give rise to the different L_s. As $2a/b$ is very small (e.g., 0.1), the contribution from the diameter possibly becomes dominant compared with that from the number (e.g., in inverse proportion to the spacing), which results in a slight increase in L_s with increasing diameter. However, the contribution from the number becomes significant when $2a/b$ is larger (e.g., 0.5 and 0.7); in this case, the diameter-dependent decrease is attributed to the reduction in the number of nanowires. For a mid-range $2a/b$ (e.g., 0.3), the contributions from the diameter and the number do not have a distinct difference. The contribution from the diameter perhaps plays a dominant role at shorter wavelengths; nevertheless, that from the number may become increasingly prominent at longer wavelengths. In fact, this case is complicated for qualitative analysis because it is not enough to interpret the reason when only the size and not the wavelength is considered, according to the quantitative description demonstrated in the theory section.

On the other hand, if we consider the same irradiation area A, the number of nanowires in the hexagonal arrays (Fig. 2) can be given by

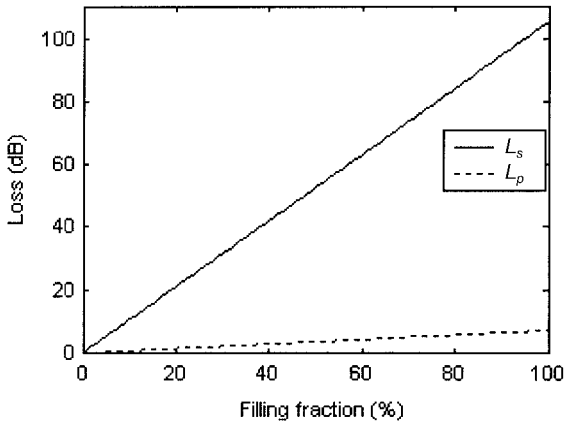

Fig. 7. Optical loss spectra with filling fraction of the nanochannels of the silver nanowire microarray at a telecommunication wavelength of 1550 nm.

$$m_p = 2\delta_m A/(\sqrt{3}b^2). \tag{20}$$

Expression (19) now has the form

$$L_R \propto \frac{A}{2\sqrt{3}}\,\delta_m\delta_l^{\,2}(2a/b)^2(a^2/\lambda^4). \tag{21}$$

When $2a/b$ is fixed, δ_m and δ_l are invariable, and we have

$$L_R \propto (a^2/\lambda^4). \tag{22}$$

Hence L_p increases when the diameter increases for a fixed value of $2a/b$ [Figs. 6(a)–6(d)]. Because the number of nanowires is uniform for the same spacing, the scattering loss can be evaluated to be proportional to a^4/λ^4. Consequently L_p obviously enhances with an increasing ratio of $2a$ to b for the same spacing.

On the basis of the analysis of the diameter-dependent polarization characteristics for the different values of $2a/b$, we see that a larger L_s and a smaller L_p can be obtained by a proper choice of $2a/b$ (e.g., 0.5), as shown in Fig. 6(c). In particular, L_s increases and L_p decreases with decreasing diameter from 65 to 35 nm. Therefore the large L_s and small L_p can be simultaneously obtained when the diameter of the nanowires for the selected $2a/b$ is reduced.

An important question concerning the design goal of a nanowire-grid polarizer is the expected tolerances of the polarization properties. We note that an Al wire-grid polarizer fabricated by electron-beam lithography exhibited an extinction ratio of 30 dB and insertion loss of 0.97 dB (loss of 20%) at an 800 nm wavelength band.[3] Recently a nanowire-grid polarizer fabricated by a nanoimprint lithography and electron-beam evaporation process achieved a high extinction ratio of 40 dB at the near-infrared spectral range (e.g., C band).[30] Zhou *et al.* successfully designed an in-fiber polarizer by using 45° tilted-fiber Bragg grating structures, and they obtained an extinction ratio of 33 dB near 1550 nm.[31] Compared with tolerances of those polarizers designed by lithography approach, expected manufacturing tolerances are extinction ratios of 40 dB and insertion losses of 0.5 dB for silver nanowire microarrays embedded in the AAM template by the self-assembly strategy (e.g., at the telecommunication wavelength of 1550 nm); in this respect >40 dB extinction ratio and <0.5 dB insertion loss are the expected tolerances at longer wavelengths. Because a slight increase in L_p and a remarkable increase in L_s with increasing filling fraction of the nanochannels are observed in Fig. 7, we can achieve the expected design goal for the fabricating tolerance by enhancing the filling fraction when selecting 0.5 for the ratio of $2a$ to b and 35 nm for the diameter.

4. Conclusions

We have theoretically explored the polarization characteristics of silver nanowire microarrays embedded in AAM templates. The Fresnel reflection and absorption from silver nanowires led to the extinction ratio and the insertion loss resulting from Rayleigh scattering from the nanowires. The optical losses were found to be strongly dependent on the diameter, the spacing, and the ratio of diameter to spacing for s and p polarizations. We can simultaneously achieve large extinction ratios and small insertion losses by selecting an appropriate $2a/b$ as well as by reducing the diameter. It is predicted that the sizes (e.g., $2a/b$ of 0.5 and $2a$ of 35 nm) may be expected to be the optimal parameters for the design of nanowire-grid polarizers at near- and mid-infrared wavelengths.

We are grateful to Fanghong Xue for helpful discussions. This work was supported by the Major Research Plan of the National Natural Science Foundation of China: Basic Research on Nano-Science and Technology (grant 90406008).

References

1. G. R. Bird and M. Parrish, "The wire grid as a near-infrared polarizer," J. Opt. Soc. Am. **50,** 886–891 (1960).
2. J. B. Young, H. A. Graham, and E. W. Peterson, "Wire grid infrared polarizer," Appl. Opt. **4,** 1023–1031 (1965).
3. H. Tamada, T. Doumuki, T. Yamaguchi, and S. Matsumoto, "Al wire-grid polarizer using the *s*-polarization resonance effect at the 0.8-μm-wavelength band," Opt. Lett. **22,** 419–421 (1997).
4. J. Guo and D. Brady, "Fabrication of thin-film micropolarizer arrays for visible imaging polarimetry," Appl. Opt. **39,** 1486–1492 (2000).
5. K. Nielsch, F. Müller, A. P. Li, and U. Gösele, "Uniform nickel deposition into ordered alumina pores by pulsed electrodeposition," Adv. Mater. **12,** 582–586 (2000).
6. M. Saito, M. Kirihara, T. Taniguchi, and M. Miyagi, "Micropolarizer made of the anodized alumina film," Appl. Phys. Lett. **55,** 607–609 (1989).
7. Y. T. Pang, G. W. Meng, Q. Fang, and L. D. Zhang, "Silver nanowire array infrared polarizers," Nanotechnology **14,** 20–24 (2003).
8. H. Hertz, *Electric Waves* (Macmillan, 1893), p. 177.
9. H. duBois and H. Rubens, "Polarization of long-wave heat rays by means of a wire grating," Ann. Phys. **35,** 243–276 (1911).
10. M. Zheng, L. Menon, H. Zeng, Y. Liu, S. Bandyopadhyay, R. D.

Kirby, and D. J. Sellmyer, "Magnetic properties of Ni nanowires in self-assembled arrays," Phys. Rev. B **62,** 12282–12286 (2000).
11. D. W. Lynch and W. R. Hunter, "Metals: comments on the optical constants of metals and an introduction to the data for several metals," in *Handbook of Optical Constants of Solids*, E. D. Palik, ed. (Academic, 1985), pp. 275–408.
12. M. Saito and M. Miyagi, "Anisotropic optical loss and birefringence of anodized alumina film," J. Opt. Soc. Am. A **6,** 1895–1900 (1989).
13. J. X. Zhang, L. D. Zhang, C. H. Ye, M. Chang, Y. G. Yan, and Q. F. Lu, "Polarization properties of ordered copper nanowire microarrays embedded in anodic alumina membrane," Chem. Phys. Lett. **400,** 158–162 (2004).
14. A. L. Prieto, M. S. Sander, M. Martin-Gonzalez, R. Gronsky, T. Sands, and A. M. Stacy, "Electrodeposition of ordered Bi_2Te_3 nanowire arrays," J. Am. Chem. Soc. **123,** 7160–7161 (2001).
15. F. Gervais, "Aluminum oxide (Al_2O_3)," in *Handbook of Optical Constants of Solids II*, E. D. Palik, ed. (Academic, 1991), pp. 761–775.
16. H. Masuda and K. Fukuda, "Ordered metal nanohole arrays made by a two-step replication of honeycomb structures of anodic alumina," Science **268,** 1466–1468 (1995).
17. X. Y. Zhang, L. D. Zhang, Y. Lei, L. X. Zhao, and Y. Q. Mao, "Fabrication and characterization of highly ordered Au nanowire arrays," J. Mater. Chem. **11,** 1732–1734 (2001).
18. H. Masuda, F. Hasegwa, and S. Ono, "Self-ordering of cell arrangement of anodic porous alumina formed in sulfuric acid solution," J. Electrochem. Soc. **144,** L127–L130 (1997).
19. P. M. Paulus, F. Luis, M. Kröll, G. Schmid, and L. J. de Jongh, "Low-temperature study of the magnetization reversal and magnetic anisotropy of Fe, Ni, and Co nanowires," J. Magn. Magn. Mater. **224,** 180–196 (2001).
20. F. Müller, A. D. Müller, M. Kröll, and G. Schmid, "Highly resolved electric force microscopy of metal-filled anodic alumina," Appl. Surf. Sci. **171,** 125–129 (2001).
21. G. Sauer, G. Brehm, S. Schneider, K. Nielsch, R. B. Wehrspohn, J. Choi, H. Hofmeister, and U. Gösele, "Highly ordered monocrystalline silver nanowire arrays," J. Appl. Phys. **91,** 3243–3247 (2002).
22. A. L. Prieto, M. Martin-Gonzalez, J. Keyani, R. Gronsky, T. Sands, and A. M. Stacy, "The electrodeposition of high-density, ordered arrays of $Bi_{1-x}Sb_x$ nanowires," J. Am. Chem. Soc. **125,** 2388–2389 (2003).
23. M. Vázquez, K. Pirota, M. Hernández-Vélez, V. M. Prida, D. Navas, R. Sanz, F. Batallán, and J. Velázquez, "Magnetic properties of densely packed arrays of Ni nanowires as a function of their diameter and lattice parameter," J. Appl. Phys. **95,** 6642–6644 (2004).
24. A. J. Yin, J. Li, W. Jian, A. J. Bennett, and J. M. Xu, "Fabrication of highly ordered metallic nanowire arrays by electrodeposition," Appl. Phys. Lett. **79,** 1039–1041 (2001).
25. D. Grujicic and B. Pesic, "Electrodeposition of copper: the nucleation mechanisms," Electrochim. Acta **47,** 2901–2912 (2002).
26. J. C. Hulteen and C. R. Martin, "A general template-based method for the preparation of nanomaterials," J. Mater. Chem. **7,** 1075–1087 (1997).
27. M. Born and E. Wolf, "Optics of metals," in *Principles of Optics*, 6th ed. (Pergamon, 1980), pp. 611–664.
28. H. C. van de Hulst, *Light Scattering by Small Particles* (Wiley, 1957), pp. 63–84.
29. A. A. Kokhanovsky, *Optics of Light Scattering Media: Problems and Solutions* (Springer, 2001), pp. 31–39.
30. J. J. Wang, W. Zhang, X. Deng, J. Deng, F. Liu, P. Sciortino, and L. Chen, "High-performance nanowire-grid polarizers," Opt. Lett. **30,** 195–197 (2005).
31. K. Zhou, G. Simpson, X. Chen, L. Zhang, and I. Bennion, "High extinction ratio in fiber polarizers based on 45° tilted fiber Bragg gratings," Opt. Lett. **30,** 1285–1287 (2005).